A Structural and Mechanistic Study of the Oxidation of Methionine Residues in hPTH(1−34) via Experiments and Simulations[†]

Jhih-Wei Chu, Jin Yin, Daniel I. C. Wang, and Bernhardt L. Trout*

Department of Chemical Engineering, Massachusetts Institute of Technology, 77 Massachusetts Avenue, Room 66-458, Cambridge, Massachusetts 02139

Received April 27, 2004; Revised Manuscript Received June 25, 2004

ABSTRACT: The relationship between the conformational properties of 1−34 human parathyroid hormone [hPTH(1−34)] and the oxidation of its methionine residues, Met8 and Met18, by hydrogen peroxide is analyzed as a function of pH by measuring the rates of oxidation and by performing MD simulations with an explicit representation of water molecules. Between pH 4 and pH 8, both Met8 and Met18 have nearly pH independent rates of oxidation, and Met18 is oxidized at a rate that is 90−100% of that of freeMet and 10−20% faster than that of Met8. We also found that average 2SWCNs calculated from MD simulations correlate well to the rates of oxidation of Met8 and Met18. The use of 2SWCNs is based on the mechanism that we proposed, the water-mediated mechanism, in which water molecules stabilize the transition state via specific interactions, but the transfer of protons (acid-catalyzed mechanism) does not play a role [Chu, J. W., and Trout, B. L. (2004) *J. Am. Chem. Soc. 126* (3), 900−908]. Only at very low pH values, pH 1 for the oxidation of freeMet, does the acid-catalyzed oxidation mechanism become important. For the oxidation of Met8 and Met18 in hPTH(1−34), the acid-catalyzed mechanism becomes significant at a higher pH value, pH 2, probably due to the proximity of nearby acidic residues to Met8 (Glu4) and Met18 (Glu22). In this study, we have demonstrated that the chemistry of oxidation and the structure of polypeptides can be correlated via a detailed understanding of the reaction mechanism, appropriate sampling of configurational space, and a suitable choice of a structural property, water coordination number.

Oxidation of methionine residues is one of the major degradation pathways of therapeutic proteins in aqueous solutions (*13*, *14*, *26*, *30*, *33*, *40*, *43*). To develop rational approaches for designing formulations that stabilize therapeutic proteins, it is essential to understand the mechanisms of degradation processes. Early studies have shown that peroxides are one of the major reactive oxygen species that cause the oxidation of proteins (*26*). The mechanism by which hydrogen peroxide, or hydroperoxides in general, oxidizes organic sulfides, such as methionine, has been elucidated recently in our laboratory by using *ab initio* calculations and molecular simulations (*10*−*12*). A summary of our conclusions is that specific interactions, such as hydrogen bonding, with surrounding water molecules stabilize the charge separation developed during the S_N2 oxidation of H_2O_2, i.e., during the breaking of the O−O bond and the formation of the S−O bond. This "water-mediated" mechanism is consistent with available experimental data such as activation energies (10−20 kcal/mol), and is significantly different from the acid-catalyzed mechanism that has been prevalent in the literature (*3*, *4*, *15*, *16*, *18*, *26*, *39*). Our mechanism is also consistent with the fact that within a medium range of pH (pH 2−10), the rates of oxidation are generally pH independent (*2*, *31*).

The water-mediated mechanism also leads to the conclusion that the access of solvent molecules to methionine sites governs oxidation. A typical property used to describe the degree to which solvent molecules can access a particular site is solvent accessible area (*25*) which is generally computed from the X-ray structure of a protein (*21*, *27*, *30*). However, in practice, the property does not provide a good measure of susceptibility to oxidation. For example, solvent accessible areas of Met122, Met127, and Met138 of granulocyte colony-stimulating factor (G-CSF) are all zero, yet all of these residues are susceptible to oxidation (*11*, *27*). On the basis of this failure of solvent accessible area, we found another molecular property that correlates well to the rates of oxidation, the ensemble average of the two-shell water coordination number (2SWCN)[1] of the sulfur atoms of methionine residues (*11*). This property thus incorporates both the dynamics of the protein and the explicit molecular simulation of water. For G-CSF, a protein with four compactly packed helices and a well-defined tertiary structure, the average 2SWCNs were shown to correlate well with the rates of oxidation of different methionine residues (*11*). Application of our approach to flexible polypeptides without a well-defined tertiary structure is one of the objectives in this study as an aid in gaining a further understanding of

[†] Funding provided by Amgen, Inc., the National University of Singapore, and the Singapore-MIT Alliance.

* To whom correspondence should be addressed. E-mail: trout@mit.edu. Telephone: (617) 258-5021. Fax: (617) 258-5042.

[1] Abbreviations: MD, molecular dynamics; hPTH(1−34), residues 1−34 of human parathyroid hormone; freeMet, free methionine amino acid; 2SWCN, two-shell water coordination number; SAA, solvent accessible area.

10.1021/bi049151v CCC: $27.50 © 2004 American Chemical Society
Published on Web 10/05/2004

the structural property−oxidation relationship of polypeptides.

In this work, we investigate the oxidation of methionine residues of a 34-residue peptide, 1−34 human parathyroid hormone [hPTH(1−34)], by hydrogen peroxide. We measure the rates of oxidation of methionine residues in hPTH(1−34) and its circular dichroism (CD) spectra as a function of pH, and also perform molecular dynamics simulations of this molecule to determine the correspondence between the conformational properties of hPTH(1−34) and the rates of oxidation of it methionine groups.

Human parathyroid hormone (hPTH) is an 84-amino acid peptide with influence on cell proliferation of skeletal tissues and on bone metabolism (*41*). It is generally accepted that the N-terminal 34-amino acid fragment of hPTH is sufficient for biological activity (*37*), and in fact, it is playing an important role in osteoporosis (*6*) and hypoparathyroidism (*45*) treatments. Compared to G-CSF (175 residues, compactly packed), hPTH(1−34) manifests significant structural variation in an aqueous solution as determined by NMR spectroscopy (*5*, *6*, *24*, *29*, *36*, *42*). hPTH(1−34) has two methionine residues, Met8 and Met18, each of which can be oxidized by H_2O_2 at a different rate (*31*). Oxidation of methionine residues has also been shown to lead to the loss of biological activity of hPTH(1−34) (*31*). These properties of hPTH(1−34) make it an important system to study to better understand the structural−oxidation relationship of polypeptides.

In the following sections, the experimental procedures for measuring the rates of oxidation of methionine residues, CD spectra, and the protocols of MD simulations are first described. We then present the results of oxidation kinetics and MD simulations with an emphasis on the correlation between structural properties and rates of oxidation. Finally, we finish with conclusions.

MATERIALS AND METHODS

Oxidation of Free Methionine. Free methionine (16 mM) was incubated with H_2O_2 (0.6 mM) in the pH range of 1−8 at 25 °C. Oxidation rate constants were determined by measuring the decrease in the H_2O_2 concentration, using a ferrous oxidation in the xylenol orange (FOX) assay as described by Wolff (*47*). The incubation buffers that were used were 100 mM HCl for pH 1, 50 mM phosphate for pH 2, 50 mM citrate for pH 3 and 4, 40 mM citrate for pH 6, and 50 mM Tris for pH 8. The ionic strengths of all buffers were adjusted to 200 mM with NaCl.

Oxidation of hPTH(1−34). hPTH(1−34) (Sigma catalog no. P-3796) was incubated with H_2O_2 (Sigma catalog no. H-1009) in the pH range of 2−8 at 25 °C [final H_2O_2 concentration of 1 mM, hPTH(1−34) concentration of 20 μM]. The incubation buffers were 50 mM phosphate for pH 2, 50 mM citrate for pH 4, 60 mM citrate for pH 6, and 50 mM Tris for pH 8. The ionic strengths of all buffers were adjusted to 0.2 M with NaCl. At various time intervals, oxidation was terminated by performing high-pressure liquid chromatography (HPLC).

Separation of Oxidized Forms of hPTH(1−34). Oxidized forms of hPTH(1−34) were separated by reverse-phase HPLC. The apparatus used was a Beckman Coulter System Gold HPLC system that includes a type 126 solvent module, a type 168 detector, and a type 508 autosampler. H_2O_2-oxidized samples (30 μL) were injected into C4 columns (Vydac 214TP52; 300 Å, 5 μm, 2.1 mm inside diameter × 25 cm). The mobile phases were solvent A [0.1% (w/v) trifluoroacetic acid (TFA)] and solvent B [0.1% (w/v) TFA in 90% acetonitrile]. The column was initially equilibrated with 20% B at a flow rate of 0.2 mL/min. After sample injection, the separation was performed with a linear gradient of 20 to 28% B for 10 min and 28 to 35% B for 70 min at a flow rate of 0.2 mL/min with the UV detector set at 215 nm.

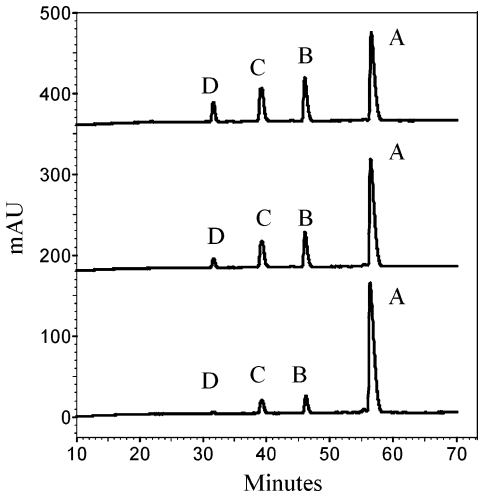

FIGURE 1: Reverse-phase HPLC for the separation of hPTH(1−34) oxidized by H_2O_2 at various oxidation times [20 mM hPTH(1−34) and 1 mM H_2O_2 at pH 4.0 and 25 °C].

Mass Spectrometry. Matrix-assisted laser desorption/ionization time-of-flight mass spectrometry (MALDI-TOF MS) was performed at the MIT Biopolymers Laboratory, using a Voyager-DETM STR BioSpectrometry Workstation (PerSpective Biosystems). Samples were dried in a Speed-Vac first and then purified with ZipTipC18 (Millipore), following the manufacturer's instruction. α-Cyano-4-hydroxycinnamic acid was used as a matrix. Measurements were taken in the positive, linear mode, and the accelerating voltage was 20 000 V.

Identification of Oxidized Forms of hPTH(1−34). The extent of oxidation of individual methionine residues in hPTH(1−34) was detected and quantified by reverse-phase HPLC. Figure 1 shows the comparison of hPTH(1−34) samples taken at 140, 380, and 620 min during H_2O_2 oxidation at pH 4.0 and 25 °C. Four distinct peaks (A−D) were obtained. Each peak was collected and subjected to mass spectrometry to measure the molecular weight of the molecule associated with it. Peak A is the intact hPTH(1−34). Peaks B−D are the oxidation products of peak A. An increase of 32 mass units, found for peak D, represents oxidation at both Met8 and Met18. Likewise, an increase of 16 mass units, found for peaks B and C, represents their oxidation at either Met8 or Met18. In addition, we used trypsin (Sigma catalog no. T8658) to cleave peak B and peak C peptides. The trypsin-cleaved peak B and peak C peptide fragments were subjected to mass spectrometry to measure their molecular weights, and the results confirmed that peak

B represents oxidation at Met18 and peak C represents oxidation at Met8.

Kinetics of Methionine Oxidation in hPTH(1−34). By assuming that unoxidized and oxidized hPTH(1−34) have similar absorbance coefficients at 215 nm, we can determine percentages of intact hPTH(1−34), hPTH(1−34) oxidized at Met8 or Met8(O), and hPTH(1−34) oxidized at both Met8 and Met18 from reverse-phase HPLC analyses, as shown in Figure 1. If we assume pseudo-first-order kinetics, the initial rate constants of Met8 and Met18 oxidation are estimated by plotting the time course of the percentage of unoxidized Met8 or Met18 with a time interval of 2 h on a semilog scale. The pseudo-first-order assumption was justified by the high linearity of the semilog plots of unoxidized Met8 and Met18 ($R^2 > 0.99$). The regression statistics indicate that the change in H_2O_2 concentration has negligible effects on the rate constants ($R^2 > 0.99$).

CD Spectroscopy. CD spectra were recorded at 20 °C in a 0.1 cm cell from 250 to 200 nm at 0.2 nm/s (four scans) on an Aviv 62 DS spectrometer. A protein concentration of 100 μM is prepared. CD spectra of hPTH(1−34) were collected at five pH values, controlled by different buffers: 100 mM HCl for pH 1, 50 mM phosphate for pH 2, 50 mM citrate for pH 4, 40 mM citrate for pH 6, and 50 mM Tris for pH 8. Ionic strengths were controlled at 200 mM using NaCl. Estimations of the helical fraction of the peptide were calculated using the value of $[\theta]_{obs}$ at 222 nm $[([\theta]^{222}_{obs} - 3000)/-39000 \times 100]$ (*36*).

Molecular Dynamics Simulations

Molecular dynamics (MD) simulations of hPTH(1−34) and analyses thereof were performed using CHARMM (*7*) with the CHARMM 22 all-atom potential (*28*). The initial configurations of hPTH(1−34) were obtained from the NMR structures of Marx *et al*. (*29*) determined at pH 6.2 (PDB entry 1ZWA) containing 10 different structures. Each structure was first solvated in a pre-equilibrated rectangular water box with at least three solvation shells from any atom of hPTH(1−34) to the box boundary. The largest box needed to satisfy this criterion contains 5326 water molecules and was used for the simulation of all structures. After the molecule had been inserted into the water box, water molecules with oxygen atoms within 2.6 Å of the atoms of hPTH(1−34) were deleted. The total system then contained 15 711 atoms and was subject to minimization before the dynamics simulation.

During the minimization calculations and MD simulations, periodic boundary conditions were applied to water molecules. Long-range electrostatic interactions were calculated via the particle mesh Ewald summation method (*17*, *19*) with a cutoff of 15 Å for real space interactions and for van der Waals interactions. Bond lengths associated with hydrogen atoms were fixed at their equilibrium values using the SHAKE algorithm (*1*), thus allowing a time step of 0.002 ps for the integration of the equations of motion. The solvated structures were first minimized by 200 steepest descent steps followed by ABNR (adopted-basis Newton−Raphson) (*7*) minimizations, until the rms (root-mean-square) force was less then 0.2 kcal mol^{-1} Å^{-1}. During the minimization steps, the backbone atoms of hPTH(1−34) were restrained to their NMR positions with a spring constant of 30 kcal mol^{-1} Å^{-1}.

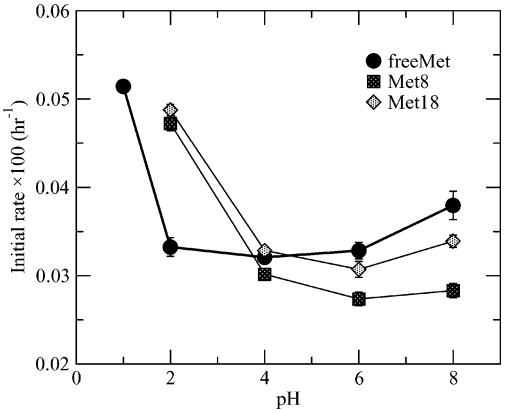

FIGURE 2: Pseudo-first-order rate constants for the oxidation of the methionine amino acid (freeMet) and methionine residues in hPTH at different pH values.

The minimized system was then brought to 300 K by assigning velocities according to Botzmann distributions with an increasing rate of 3 K/0.1 ps for 10 ps. After being heated, the system was coupled to a Langevin piston (*48*) to hold the system pressure at 1 atm and a Nosé-Hoover thermostat (*34*) to hold the temperature at 300 K. The simulations were then continued for 2.04 ns. To sample the conformation of hPTH(1−34) more efficiently, separate 2.05 ns MD simulations started from each of the 10 reported NMR structures were performed, instead of one long simulation started from one of the NMR structures (*9*). Simulation results with only one of the side chain nitrogens protonated are denoted as "high-pH" (net charge of 1); when both nitrogen atoms of histidine residues are protonated, the results are denoted as "medium-pH" (net charge of 4). The same procedures were applied to all simulations performed in this study. If not otherwise mentioned, statistics reported in this study are taken from the last 1 ns of each simulation. Statistical uncertainties of each simulation were estimated by using the standard asymptotic block-averaging method (*1*, *20*).

The water coordination number is defined as the number of water molecules within a cutoff region around a specified atom, for example, the sulfur atom of a methionine residue. The choice of a cutoff radius to describe the oxidation rates is 5.5 Å (2SWCN). The rationale behind this option is that water molecules surrounding hydrogen peroxide participate the reaction via specific interactions such as hydrogen bonding. Such interactions are needed to stabilize the charge separation during the S_N2 oxidation by H_2O_2 (*10*). To capture the effects of water molecules surrounding the reactants (the sulfur atom and H_2O_2), two solvation shells are used and indeed perform better in correlating the rates of oxidation than different cutoff radii (*11*).

RESULTS AND DISCUSSION

Rates of Oxidation of Met8 and Met18 at Different pH Values

The measured initial rates of oxidation of free methionine (freeMet), Met8, and Met18 as a function of pH are shown in Figure 2. The rates of oxidation of freeMet do not depend on pH significantly between pH 2 and 8, another validation of the water-mediated mechanism that we proposed for oxidation (*10*, *11*). The rate of oxidation of freeMet, however, jumps significantly when the pH is lowered to 1. We attribute

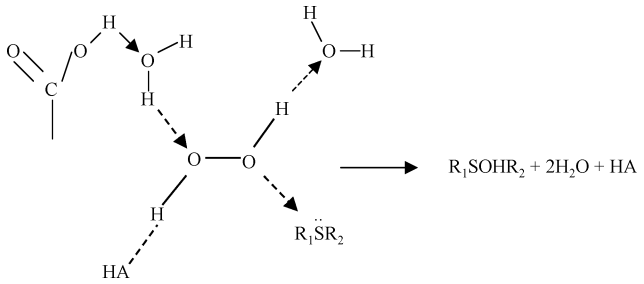

FIGURE 3: Proposed the acid-catalyzed mechanism in the presence of a protonated acidic residue at low pH values. In the acid-catalyzed mechanism, a protonated solvent molecule is needed (*33*), and at low pH values, a surrounding acidic residue can provide the additional proton. A carbonyl oxygen at a distance of two to three solvation shells from the sulfur atom suffices for this purpose.

this increase to the manifestation of the acid-catalyzed mechanism proposed by Bach *et al.* (*3*) in which a protonated water molecule serves as the general acid for the oxidation of dimethyl sulfide (DMS). This acid-catalyzed mechanism becomes important as the concentration of hydronium ions become large, and an increase of the rates of oxidation of DMS at pH 1 compared to those at pH 2 has been also been observed (*2*), consistent with the oxidation of freeMet shown in Figure 2. For the oxidation of methionine in protein formulations, however, the acid-catalyzed mechanism is not relevant but the water-mediated mechanism becomes important since the rates of oxidation of methionine are not a strong function of pH between pH 2 and 8.

For the oxidation of methionine residues in hPTH(1−34) above pH 2, Met18 is oxidized at a rate that is 90−100% of that of freeMet, and Met8 is oxidized 10−20% slower than Met18. The rates of oxidation of both Met8 and Met18 are not very sensitive to pH for pH >2, as is the case for freeMet. The small difference in the rates of oxidation between Met8 and Met18 indicates that the local environments around these two residues are only slightly different. These differences will be examined later. At pH 2, however, both Met8 and Met18 are oxidized faster than freeMet, and the rate of oxidation of each is close that of freeMet at pH 1. This result indicates that the acid-catalyzed mechanism becomes significant in hPTH(1−34) at a slightly higher pH value than in freeMet. This observation is most likely to be due to the proximity of the glutamic acid residues (Glu) to the methionine resides, Met8 (Glu4) and Met18 (Glu22). Glu residues within 10 Å of the active site are known to serve as proton pumps in enzymatic reactions that involve proton transfer and have been identified as the key residues in maintaining the activity of a number of enzymes (*8*, *22*, *35*, *44*). For the case of oxidation, a schematic representation of the acid-catalyzed oxidation mechanism near an acidic group is shown in Figure 3. hPTH(1−34) has a total of four acidic residues, including Glu4, which is near Met8 in the N-terminal helix, and Glu19 and Glu22, which are near Met18 in the C-terminal helix (see Figure 4). The CD spectra, which will be presented later, indicate that the helical content of hPTH(1−34) is independent of pH, and molecular dynamics simulations demonstrate that the distances between the carboxylic oxygen atoms of Glu4 and Glu22 and the sulfur atoms of Met8 and Met18 are <7.0 Å in the helical structure of the N- and C-termini. Therefore, the effective concentration of protons around Met8 and Met18 of hPTH(1−34) should be higher than that around freeMet at pH 2 (pK_a of Glu = 4), and this increased concentration likely results in a more significant effect of the acid-catalyzed mechanism at pH 2. Note that there are no acidic residues in the proximity of Met1 in G-CSF, the protein studied in our previous paper (*11*), and this residue has a rate of oxidation lower than that of freeMet at pH 2 (*10*). For most practical situations, however, the acid-catalyzed mechanism will not be important, since the range of pH values that is usually used in the formulation of protein pharmaceuticals is pH 4.5−7.5 (*38*), where the water-mediated mechanism is most relevant.

FIGURE 4: Ribbon representation of 1ZWA-2, the second of the selected NMR structures (PDB entry 1ZWA). Glu4 and Met8, and Met18 and GLu22, are shown in black. Note that the distances between Glu4 and Met8 and between Met18 and Glu22 are around 5.5 Å.

Structural Properties of hPTH(1−34) and Rates of Oxidation of Met8 and Met18

Now we start to address the relationship between the rates of oxidation of the methionine residues of hPTH(1−34) and the structural properties of the peptide in the range of pH values where the water-mediated oxidation mechanism is dominant (pH 4−8). In addition to CD spectra, the configuration space of hPTH(1−34) in solution is also explored by performing MD simulations according to the protocols described earlier. We first present the results of CD spectra and MD simulations. The correspondence between the structural properties of hPTH(1−34) and the rates of oxidation of Met8 and Met18 is then examined by using the two-shell water coordination number (2SWCN), which has been shown previously to correlate well to the rates of oxidation of methionine residues in G-CSF (*11*).

CD Spectra. hPTH(1−34) has many chargeable residues, including three His residues (His9, His14, and His32), four acidic residues (Glu4, Glu19, Glu22, and Asp30), and five basic residues (Lys13, Arg20, Arg25, Lys26, and Lys27). Therefore, the intramolecular electrostatic interactions are expected to play important roles in the structure of hPTH(1−34). Indeed, it has been shown that increasing the ionic strength results in an slight increase in the helicity of hPTH(1−34) (from 24 to 28%) (*36*).

The measured ellipticity of hPTH(1−34) at different pH values is shown in Figure 5, and the estimated helical fraction of hPTH(1−34) as a function of pH is shown in Figure 6. It can be seen that the helical content of hPTH(1−34) is around 23%, independent of pH from pH 1 to 8, and this is close to the value reported in an earlier study, 24%, at pH 6.3 (*36*). These data suggest that the secondary structure of hPTH(1−34) does not change even under acidic conditions, implying that the conformational properties are not sensitive to pH. This result is also consistent with the result that the oxidation rates are not sensitive to pH in the range of 4−8, according to the water-mediated oxidation mechanism. It also adds further confirmation of our theory that the increases in

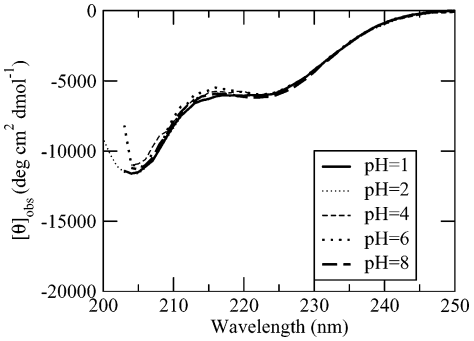

FIGURE 5: Measured ellipticity of hPTH(1−34) as a function of pH.

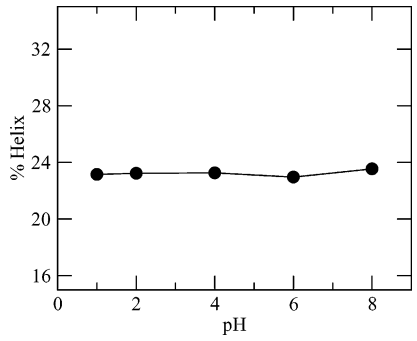

FIGURE 6: Helix fraction of hPTH(1−34) as a function of pH estimated via the measured ellipticity from CD spectroscopy; % helix = $([\theta]^{222}_{obs} - 3000)/(-39000 \times 100)$ (*36*).

the rates are due to the acid-catalyzed mechanism coming into play. Note that the helical content of G-CSF, which has a well-defined tertiary structure, is sensitive to pH (*32*), and thus, the rate of oxidation of methionine groups in G-CSF is a function of pH, even in the intermediate ranges of pH, when solely the water-mediated mechanism is important.

MD Simulations of hTPH(1−34) and Its Conformational Properties. While some studies indicate that hPTH(1−34) has a short N-terminal helix from Gln6 to His9, and a longer C-terminal helix from Met18 to Gln29 connected by a flexible hinge around Gly12, the secondary structures of hPTH(1−34) are not strictly regular, but are flexible and consist of extended or irregular structures (*29*, *36*). For example, the chemical shifts of the residues in the N-terminal helix are only marginally lower than those of a random coil (*29*, *36*), and the α-helical Hα(*i*)−HN(*i* + 3) NOEs are low intensity NOEs when *i* = 6 in the N-terminal helix and when *i* = 24 or 26 in the C-terminal helix (*36*). Indeed, the number of residues with helical NOE signals is around 17 (*29*), but the CD spectra only suggest the presence of eight helical residues. Moreover, distance geometry calculations also indicate that a single structure cannot fulfill all of the experimental restraints, suggesting the existence of both structured and unstructured peptide structures in an aqueous solution (*36*). hPTH(1−34) also has very few long-range NOE signals, a further indication of its flexibility, and the major long-range interactions identified by NMR spectroscopy are between the δ-protons of Leu15 and the aromatic protons of Trp23, both hydrophobic. On the basis of the looseness of the structure on this molecule, we chose to study the 10 most representative structures determined via matching NOE constraints measured at pH 6.3 (*29*) (PDB entry 1ZWA). Each structure is denoted as 1ZWA-*i* (*i* = 1−10 in this work).

The 10 structures can be roughly clustered into four groups based on the overall folding as determined by geometrical quantities, such as the radius of gyration. Ribbon representations of these structures are shown in Figure 7. Since the 10 structures are very distinct from one another, we report both the properties of each structure and the average properties of all 10 structures. In the following sections, Avg will be placed in front of a property if it is averaged over the properties of the 10 structures.

The root-mean-square deviations (rmsds) of α-carbons in each MD trajectory are computed with respect to the NMR structure. The average of all 10 of these rmsds is 4.8 ± 0.9 Å for high pH and 5.2 ± 0.76 Å for medium pH. The fairly large α-carbon rmsds indicate that hPTH(1−34) indeed is flexible and deviates significantly from the starting NMR structures during the period of the 2 ns simulations. Although the rmsd of each simulation is large, analyses of the cross rmsds (rmsds of the trajectory of 1ZWA-*j* with respect to the starting structure of 1ZWA-*i*) indicate that each simulation is more similar to its own starting structure than to other NMR structures. This nonergocity of MD simulations of polypeptides has been reported (*9*), and we use the approach of performing multiple simulations with different initial structures, instead of running a long trajectory starting from a single configuration.

The NMR structures of hPTH(1−34) were determined by Marx *et al*. via 207 NOEs using constrained MD simulations and simulated annealing techniques (*29*). We computed the percentage of time that NOEs are satisfied during the last 1 ns of a trajectory, and present the results in Table 1. The criteria for satisfying the constraints depend on the relative intensities (*29*): 2.0−4.0 Å for high-intensity NOEs, 2.0−5.0 Å for medium-intensity NOEs, and 2.0−5.5 Å for low-intensity NOEs. The NOEs can be divided into three categories: short range which includes *i* + 1 and *i* + 2 NOEs (total of 127), medium range which includes *i* + 3, *i* + 4, and *i* + 5 NOEs (total of 75), and long range for $>i + 5$ [observed in hPTH(1−34) only between Leu15 and Trp23].

As shown in Table 1, more than 60% of the short-range NOEs are satisfied in each trajectory and the average is 69% for both high-pH and medium-pH simulations. For medium-range NOEs, however, the percentages vary significantly among different NMR structures, and the average is around 40% in high- and medium-pH simulations. Since the medium-range NOEs are closely related to helical secondary structures, this result of MD simulations indicates that the helical structures of hPTH(1−34) have significant variation in an aqueous solution, consistent with the results of earlier NMR studies (*29*, *36*). Although only 40% of medium-range NOEs are satisfied, the number of helical residues identified using the DSSP program (*23*) still has an average value of around 12, as shown in Table 1. Note also that in the reported NMR structures (*29*), the average number of helical residues is 16, but CD spectra only suggest the existence of eight helical residues. These results indicate that not all NOEs related to the helical structures are satisfied in an aqueous environment. This is similar to the conclusion of earlier distance geometry calculations (*36*) on hPTH(1−34).

The Leu15−Trp23 interactions have been observed at both pH 6 and 4 via NMR spectroscopy (*6*, *29*, *36*). In the MD simulations, an average of 57% of the 10 trajectories exhibit the Leu15−Trp23 interaction in the high-pH simulations and

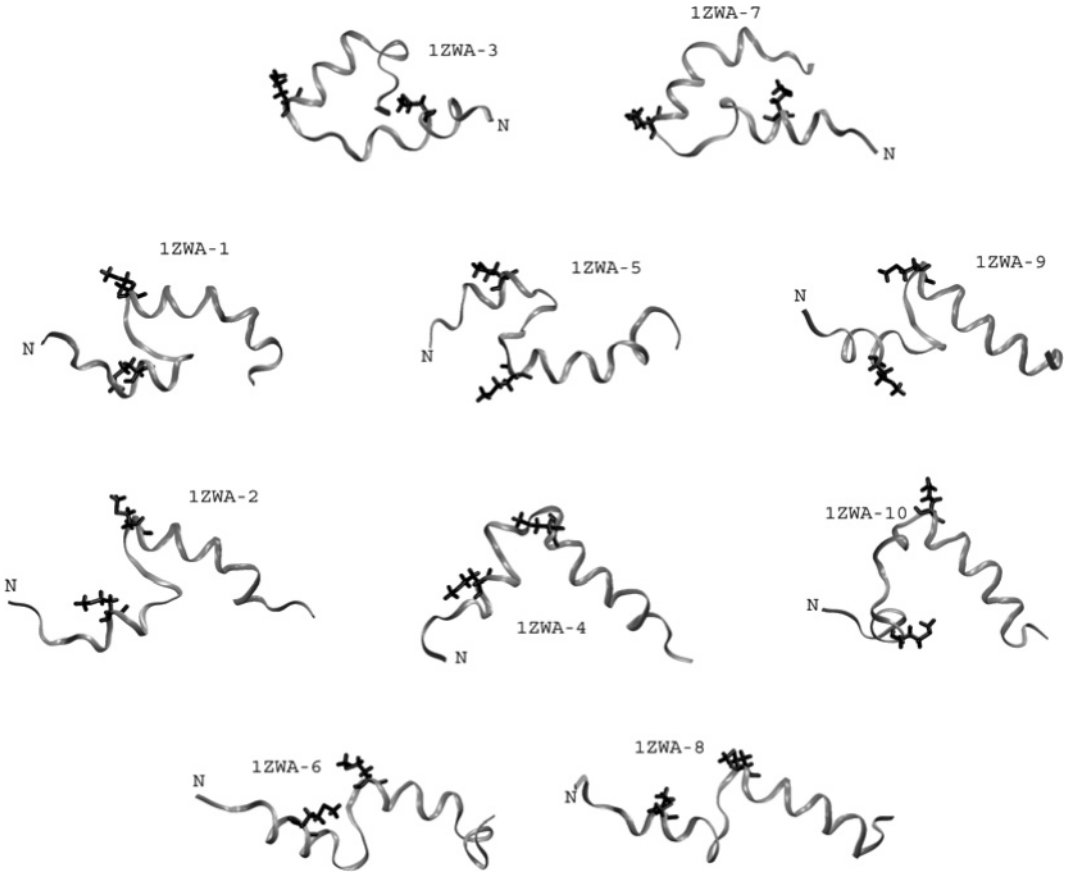

FIGURE 7: Ribbon representations of NMR structures of hPTH(1−34) (PDB entry 1ZWA). Each structure is labeled as 1ZWA-*i* ($i = 1-10$). The 10 NMR structures are roughly clustered into four groups ($i = 3$ and 7, $i = 1$, 5, and 9, $i = 2$, 4, and 10, and $i = 6$ and 8). The groups are listed in ascending order according to the value of the radius of gyration of their α-carbons. Met8 and Met18 are shown in black, and the location of the N-terminus is labeled with an N.

Table 1: Percentage of Time that the Various NOE Constraints Are Satisfied in the MD Trajectories

	short-range[a]		medium-range[b]		helical residues[c]		Leu15−Trp23[d]	
simulation	high[e]	medium[f]	high	medium	high	medium	high	medium
1ZWA-1	71	69	52	37	13.21	12.81	87	93
1ZWA-2	68	69	39	35	10.54	9.52	28	75
1ZWA-3	69	69	27	37	8.66	8.49	88	100
1ZWA-4	70	71	55	42	14.81	13.86	100	0
1ZWA-5	74	74	44	52	13.63	11.93	81	2
1ZWA-6	67	67	53	37	19.63	11.22	89	95
1ZWA-7	70	68	12	25	3.29	12.74	0	25
1ZWA-8	70	68	52	48	14.76	11.94	100	9
1ZWA-9	62	62	34	21	9.69	10.22	0	5
1ZWA-10	70	68	53	42	12.85	12.62	0	57
average-1[g]	69	69	42	38	12.11	11.53	57	46

[a] Percentage of $i + 1$ and $i + 2$ NOEs (127 in total) that are satisfied by a trajectory. [b] Percentage of $i + 3$, $i + 4$, and $i + 5$ NOEs (75 in total) that are satisifed by a trajectory. [c] Average number of helical residues in a trajectory identified via DSSP (*23*). [d] Percentage of a trajectory with long-range interactions between Leu15 and Trp23 (three NOEs). [e] Only one side chain nitrogen of histidine is protonated. [f] Two side chain nitrogens of histidine are protonated. [g] Average over 10 simulations.

46 in the medium-pH simulations. As for the medium-range NOEs, the Leu15−Trp23 interaction has very different values over the 10 simulations due to the structural diversity of hPTH(1−34). Although the Leu15−Trp23 NOEs are not satisfied in a significant percent of the trajectories, in most of these trajectories, the amount by which the distances exceeds the NOE constraint is below 2.0 Å, and only one of the 10 trajectories has an average violation of >6 Å (1ZWA-9 at high pH and 1ZWA-4 at medium pH). Therefore, we conclude that long-range interactions exist between Leu15 and Trp23 in the MD simulations. Note also that there does not exist a clear trend between the medium-range NOEs, which are related to the helical structures, and the Leu15−Trp23 interactions. For example, 1ZWA-3 in both the high-pH and medium-pH simulations exhibits strong Leu15−Trp23 interactions (Table 1) but has relatively weak medium-pH NOEs. On the other hand, for 1ZWA-8 in the medium-pH simulations, the percentage of satisfied medium-range NOEs is above average, but the Leu15−Trp23 interaction is very weak.

To understand more about the structural variation of hPTH(1−34) in an aqueous solution, we plot the local rmsd (lrmsd) of α-carbons with respect to NMR structures with a five-amino acid window (*46*) (Figure 8). The results dem-

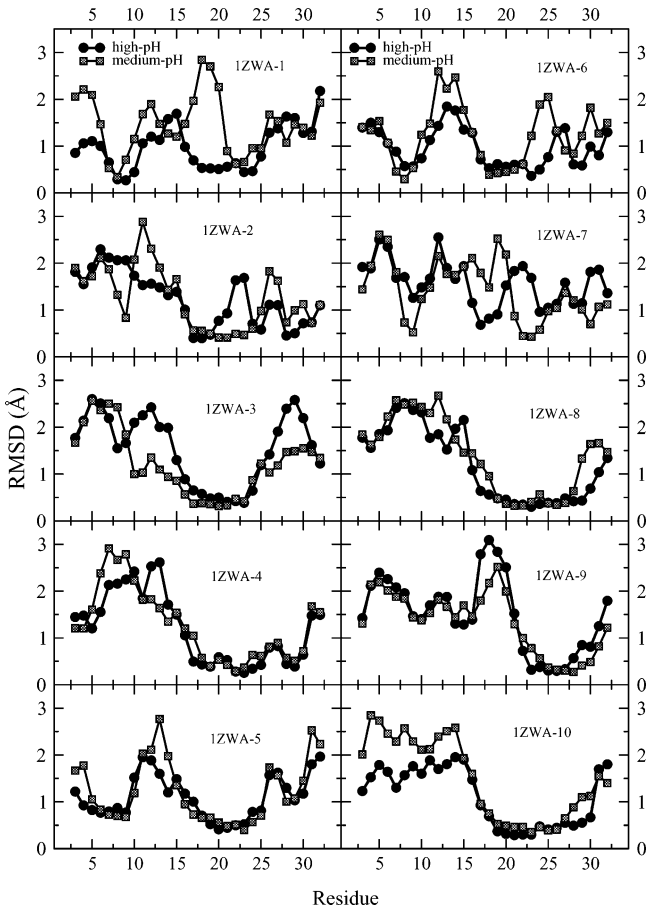

FIGURE 8: Local rmsd (with respect to the NMR structures) of α-carbons with a five-amino acid window, averaged over the last 1 ns of each MD simulation.

onstrate that the N-terminal, C-terminal, and hinge (around Gly12) regions of hPTH(1−34) are generally more flexible than the helical regions. The lrmsds of residues 19−29 are small (<1 Å) in most simulations, indicating that the C-terminal helix is quite stable. Large lrmsds (>1.5 Å) that occur in the C-terminal helix regions in some of the 10 simulations usually involve residues in the beginning of the helix (around Glu19) or around the middle of the C-terminal helix (Glu22 or Arg25) and are consistent with the observation that the helical NOEs around this region are weak (*36*). The N-terminal helix, however, is less stable in the MD simulations than what would be expected from the NMR structures. In the cases of large lrmsds (>1.5 Å) in the N-terminal helix region, residues 6−9, the helicity is usually lost. This leads to the smaller numbers of helical residues in MD simulations as shown in Table 1. The results given above suggest that the N-terminal helix can indeed exist in irregular structures as reported in the NMR studies (*29*, *36*).

In summary, the results of MD simulations are consistent with the structural properties of hPTH(1−34) observed via NMR spectroscopy and CD spectra; i.e., hPTH(1−34) has a short helix in the N-terminus (residues 6−9) but may exhibit an unstructured or irregular conformation, has a longer helix (19−29) in the C-terminus that is more stable, and has long-range interactions between hydrophobic residues Leu15 and Trp23. Moreover, we did not observe a strong dependence of the above properties on the degree of protonation of the histidine residues, i.e., high-pH versus medium-pH simulations, indicating that the structural properties of hPTH(1−34) are not sensitive to pH, as was suggested by the CD spectra shown in Figure 6.

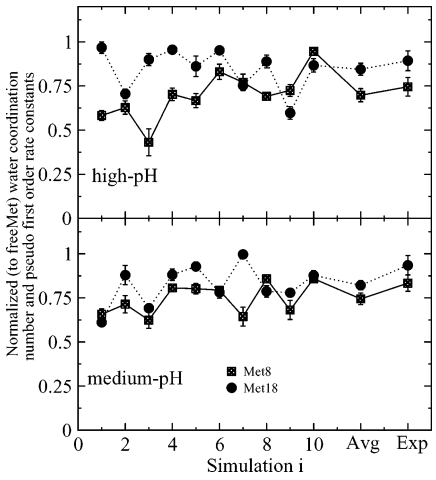

FIGURE 9: Two-shell WCNs (normalized to the value of freeMet) of Met8 and Met18 of hPTH(1−34) for each MD simulation. The *x*-axis is the identity of the starting structure (1−10), and the *y*-axis is the normalized water coordination number. The average of the values over the 10 structures is denoted Avg, and the measured rates normalized to the value of freeMet are denoted Exp. For high pH, the rates at pH 8 of Figure 2 are plotted, and for medium pH, the rates at pH 6 are plotted.

Characterization of Solvent Configuration and Correlation with the Rates of Oxidation of Met8 and Met18. In this section, we use the 2SWCN, found to correlate well to the rates of oxidation of methionine in G-CSF, to investigate hPTH(1−34).

The 2SWCNs of the sulfur atoms of Met8 and Met18 averaged over the last 1 ns of each simulation are normalized to the value of freeMet and are shown in Figure 9. On the *x*-axis, the NMR structures (Figure 9) from which a simulation is started are labeled by the integer *i*, i.e., 1ZWA-*i* ($i = 1-10$). The average over the 10 simulations, denoted as Avg on the *x*-axis of Figure 9, and the normalized rates of oxidation (to the rates of freeMet) measured experimentally (Figure 2) are also plotted in Figure 9, and are denoted Exp. The rates of oxidation of freeMet, Met8, and Met18 measured at pH 8 are compared with the results from the high-pH simulations, and the rates measured at pH 6.3 were compared with the results from the medium-pH simulations.

It can be seen from Figure 9 that in most of the high-pH simulations, Met18 has a larger 2SWCN than Met8, except for 1ZWA-7 and 1ZWA-9. Among the medium-pH simulations, only 1ZWA-1 and 1ZWA-8 have 2SWCNs that are in the order opposite from the order of oxidation rates. Figure 9 also shows that the results are very different from one trajectory to another in both medium-pH and high-pH simulations, indicating that hPTH(1−34) indeed is flexible and exhibits diverse structures. Figure 9 also demonstrates that the 2SWCNs of the sulfur atom of methionine sites are very sensitive to the conformation of the protein molecule and describe the solvent exposure of methionine sites quite well. Although there is significant variation of the 2SWCNs among the 10 simulations, the average values correspond to the measured rates of oxidation for both Met8 and Met18. The average values of the 2SWCNs and the oxidation rates are given in Table 2. Both the rates of oxidation and the 2SWCNs of Met8 and Met18 are not sensitive to pH between pH 4 and 8. The 2SWCNs have a general trend of slightly

Table 2: Normalized Two-Shell Water Coordination Numbers and Normalized Rates of Oxidation of Met1 and Met18

	Met8/Met18[a]		Met8/freeMet[b]		Met18/freeMet[c]	
pH	Exp[d]	Avg[e]	Exp	Avg	Exp	Avg
4	0.92 ± 0.01		0.94 ± 0.01		1.02 ± 0.01	
6[f]	0.89 ± 0.05	0.92 ± 0.07	0.83 ± 0.05	0.74 ± 0.03	0.94 ± 0.05	0.82 ± 0.03
8[g]	0.83 ± 0.04	0.82 ± 0.06	0.75 ± 0.05	0.7 ± 0.03	0.89 ± 0.06	0.93 ± 0.03

[a] Ratio of Met8 to Met18. [b] Ratio of Met8 to freeMet. [c] Ratio of Met18 to freeMet. [d] Measured rates of oxidation (Figure 2). [e] Average over all of the simulations. [f] The simulation results in this row are from medium-pH simulations. [g] The simulation results in this row are from high-pH simulations.

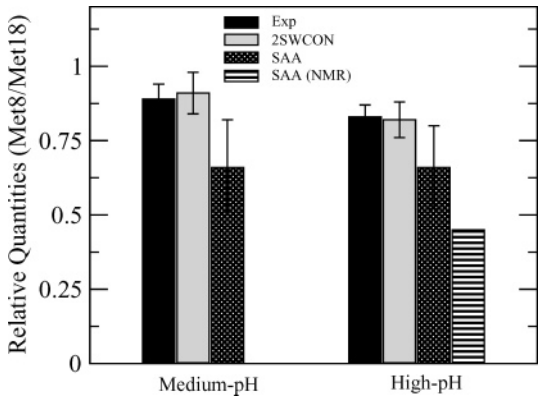

FIGURE 10: Comparison of relative properties of oxidation between Met8 and Met18. The measured rates of oxidation are denoted Exp. The average of two-shell WCNs is denoted 2SWCN. The average of solvent accessible areas is denoted SAA. The average of solvent accessible areas of the NMR structures is denoted SAA (NMR). A probe radius of 1.6 Å was used to calculate SAAs. For high pH, the quantities at pH 8 of Figure 2 are plotted, and for medium pH, the quantities at pH 6 are plotted.

underestimating the normalized rates of oxidation, but the ratios between Met8 and Met18 are very close to the experimental ratios. Therefore, even the small difference between the oxidation rates of Met8 and Met18 can still be captured by using 2SWCNs.

However, in comparison to the solvent accessible area (SAA), a property which is often used as a measure of the solvent accessibility of atoms (*25*), 2SWCNs are much better correlated to oxidation rates. In Figure 10, the relative rates of oxidation, 2SWCNs, SAAs, and SAAs of the NMR structures are compared. It can be seen that 2SWCNs provide a more accurate representation of the rates of oxidation. Similar results have also been found in the oxidation of G-CSF (*11*). Note also that determining ensemble averages from MD simulations has already significantly improved the correlation to oxidation rates of using the NMR structures. Therefore, including dynamics and an explicit reorientation of water structure is important in predicting the relative rates of oxidation of methionine.

From our simulation results, we can also explain the reason for the small differences in the rates of oxidation of Met8 and Met18. Met18 of hPTH(1−34) is located in the beginning of the C-terminal helix and right after the loop between Asn10 and Asn16. Since interactions exist between Leu15 and Trp23 and since the C-terminal helix is generally stable, the side chain of Met18 is, for most of the time, exposed to solvent (see also Figure 7). Met8, on the other hand, is located in the more flexible N-terminal helix and is not in the Leu15−Trp23 region. Therefore, the side chain of Met8 can interact with the rest of the peptide more frequently (see also Figure 7), leading to lower 2SWCNs and, thus, slower oxidation rates compared to those of Met18. For example, for a structure like 1ZWA-3 as shown in Figure 7, Met8 would have a small 2SWCN. Indeed, as shown in Figure 9, Met8 of 1ZWA-3 has a small 2SWCN compared to Met18 and 2SWCNs of Met8 in other high-pH simulations.

CONCLUSIONS

(1) The oxidation of free methionine by H_2O_2 proceeds at rates that are nearly independent of pH from pH 2 to 8, as explained by our water-mediated mechanism. At pH 1, the acid-catalyzed mechanism starts to become significant, leading to an increase in the rate of oxidation. Of course, protein formulations generally have moderate ranges of pH, and thus, for them, the water-mediated mechanism will be relevant.

(2) Both Met8 and Met18 of hPTH(1−34) can be oxidized at different rates in an aqueous solution. Met18 is oxidized 10−20% faster than Met8, and both are oxidized more slowly than free methionine between pH 4 and 8. The rates of oxidation of Met8 and Met18 are also nearly pH independent between pH 4 and 8, but at pH 2, the rates of oxidation increase. We explain this increase by an enhanced concentration of hydronium ions caused by the proximate Glu residues. These ions can exchange with the acidic residues very close to Met8 and Met18, effectively enhancing the local concentration of protons.

(3) The structural property 2SWCN indicates that the local environments of Met8 and Met18 are not sensitive to pH between pH 4 and 8, and CD spectra also show that hPTH(1−34) has a constant helical content of 23% over this pH range. These results together are consistent with our water-mediated mechanism of oxidation, for which protein conformation governs oxidation, not acidity.

(4) The rates of oxidation of Met8 and Met18 correlate to the two-shell water coordination number obtained by averaging results from MD simulations on structures obtained from NMR data. Met8 is far from the long-range interaction between Leu15 and Trp23 and is located in the flexible N-terminal helix, and Met18 is the starting residue of the C-terminal helix. Met8, thus, has frequent contacts with other residues in the peptide, lowering its exposure to solvent, while Met18 is generally exposed to solvent due to the interactions between Leu15 and Trp23. Therefore, the 2SWCN of Met8 is less than that of Met18, leading to Met8 having a lower oxidation rate than Met18.

(5) To compute properly averaged properties, it is essential to sample the dynamics of molecules over both local configurations, for example, molecular dynamics, and to perform different simulations with different initial conditions taken from NMR studies. Also, explicitly including water is essential.

(6) The relationship between conformational properties and rates of oxidation has been made for a flexible peptide, hPTH(1−34), via extensive sampling of the configurational space of hPTH(1−34). This result is based on the water-mediated mechanism that we developed, and it, thus, can be employed to better understand how different sites in proteins are susceptible to oxidation to varying degrees. This is particularly important in the development of formulations for therapeutics proteins.

ACKNOWLEDGMENT

We greatly thank Professor Amy E. Keating and Mrs. Christina Taylor at the Massachusetts Institute of Technology for helping us with the CD experiments. We also thank Dr. Bernard R. Brooks at the National Institutes of Health (Bethesda, MD), Professor Bruce Tidor at Massachusetts Institute of Technology, Dr. Wenning Wang at Fudan University (Shanghai, China), and Dr. Margaret Speed Ricci and Dr. David Brems at Amgen Inc. for helpful discussions. We also acknowledge Dr. Ute C. Marx at Universitaet Bayreuth (Bayreuth, Germany) for providing us with her NOE data of hPTH(1-34).

REFERENCES

1. Allen, M. P., and Tildesley, D. J. (1987) *Computer Simulation of Liquids*, Oxford, New York.
2. Amels, R., Elias, H., and Wannowius, K. J. (1997) Kinetics and mechanism of the oxidation of dimethyl sulfide by hydroperoxides in aqueous medium study on the potential contribution of liquid-phase oxidation of dimethyl sulfide in the atmosphere, *J. Chem. Soc., Faraday Trans. 93* (15), 2537−2544.
3. Bach, R. D., Su, M. D., and Schlegel, H. B. (1994) Oxidation of amines and sulfides with hydrogen peroxide and akyl hydrogen peroxide, *J. Am. Chem. Soc. 116*, 5379−5391.
4. Bach, R. D., Owensby, A. L., Gonzalez, C., Schlegel, H. B., and McDouall, J. (1991) Nature of the transition structure for oxygen atom transfer from a hydroperoxide. Theoretical comparison between water oxide and ammonia oxide, *J. Am. Chem. Soc. 113*, 6001−6011.
5. Barden, J. A., and Cuthbertson, R. M. (1993) Stabilized NMR structure of human parathyroid hormone(1−34), *Eur. J. Biochem. 215* (2), 315−321.
6. Barden, J. A., and Kemp, B. E. (1993) NMR solution structure of human parathyroid hormone(1−34), *Biochemistry 32* (28), 7126−7132.
7. Brooks, B. R., Bruccoleri, R. E., Olafson, B. D., States, D. J., Swaminathan, S., and Karplus, M. (1983) Charmm: A program for macromolecular energy, minimization, and dynamics calculations, *J. Comput. Chem. 4* (2), 187−217.
8. Butland, G., Spiro, S., Watmough, N. J., and Richardson, D. J. (2001) Two conserved glutamates in the bacterial nitric oxide reductase are essential for activity but not assembly of the enzyme, *J. Bacteriol. 183* (1), 189−199.
9. Caves, L. S. D., Evanseck, J. D., and Karplus, M. (1998) Locally accessible conformations of proteins: Multiple molecular dynamics simulations of crambin, *Protein Sci. 7* (3), 649−666.
10. Chu, J. W., and Trout, B. L. (2004) On the mechanisms of oxidation of organic sulfides by H_2O_2 in aqueous solutions, *J. Am. Chem. Soc. 126* (3), 900−908.
11. Chu, J. W., Yin, J., Wang, D. I. C., and Trout, B. L. (2004) Molecular dynamics simulations and oidation rates of methionine residues of granulocyte colony-stimulating factor at different pH values, *Biochemistry 43* (4), 1019−1029.
12. Chu, J. W., Brooks, B. R., and Trout, B. L. (2004) QM/MM and free energy simulations of the oxidation of methionine residues in aqueous solutions, free methionine and methionine in g-csf, *J. Am. Chem. Soc*. (submitted for publication).
13. Cleland, J. L., and Langer, R. (1994) Formulation and delivery of proteins and peptides, *ACS Symp. Ser.*, 1−19.
14. Cleland, J. L., Powell, M. F., and Shire, J. (1993) The development of stable protein formulations: A close look at protein aggregation, deamidation, and oxidation, *Crit. Rev. Ther. Drug Carrier Syst. 10* (4), 307−377.
15. Curci, R., DiPrete, R. A., Edwards, J. O., and Mondena, G. J. (1970) Role of solvent in the oxidation of some organic compounds by peroxyacids, *J. Org. Chem. 35*, 740.
16. Dankleff, M. A. P., Ruggero, C., Edwards, J. O., and Pyun, H. Y. (1968) The influence of solvent on the oxidation of thioxane by hydrogen peroxide and by *tert*-butyl hydroperoxide, *J. Am. Chem. Soc. 90*, 3209.
17. Darden, T., York, D., and Pedersen, L. (1993) Particle mesh ewald: An N*log(N) method for ewals sums in large systems, *J. Chem. Phys. 93* (12), 10089−10092.
18. Edwards, J. O. (1960) Nucleophilic displacement on oxygen in peroxides, in *Peroxide Reaction Mechanisms* (Edwards, J. O., Ed.) pp 67−106, Interscience Publishers, NewYork.
19. Essmann, U., Perers, L., Berkowitz, M. L., Darden, T., Lee, H., and Pedersen, L. G. (1995) A smooth particle mesh ewald method, *J. Chem. Phys. 103* (19), 8577−8593.
20. Frenkel, D., and Smit, B. (1996) *Understanding Molecular Simulation, From Algorithms to Applications*, Academic Press, New York.
21. Griffiths, S. W., and Cooney, C. L. (2002) Relationship between protein structure and methionine oxidation in recombinant human α-1-antitrypsin, *Biochemistry 41* (20), 6245−6252.
22. Hulett, M. D., Hornby, J. R., Ohms, S. J., Zuegg, J., Freeman, C., Gready, J. E., and Parish, C. R. (2000) Identification of active-site residues of the pro-metastatic endoglycosidase heparanase, *Biochemistry 39* (51), 15659−15667.
23. Kabsch, W., and Sander, C. (1983) Dictionary of protein secondary structure: pattern recognition of hydrogen-bonded and geometrical features, *Biopolymers 12*, 2577−2637.
24. Klaus, W., Dieckmann, T., Wray, V., Schomburg, D., Wingender, E., and Mayer, H. (1991) Investigation of the solution structure of the human parathyroid-hormone fragment (1−34) by NMR spectroscopy, distance geometry, and molecular-dynamics calculations, *Biochemistry 30* (28), 6936−6942.
25. Lee, B., and Richards, F. M. (1971) The interpretation of protein structures: Estimation of static accessibility, *J. Mol. Biol. 55*, 379−400.
26. Li, S., Schöneich, C., and Borchardt, R. T. (1995) Chemical instability of protein pharmaceuticals: Mechanisms of oxidation and strategies for stablization, *Biotechnol. Bioeng. 48*, 490−500.
27. Lu, H. S., Fausset, P. R., Narho, L. O., Horan, T., Shinagawa, K., Shimamoto, G., and Boone, T. C. (1999) Chemical modification and site-directed mutagenesis of methionine residues in recombinant human granulocyte colony-stimulating factor: Effect on stability and biological activity, *Arch. Biochem. Biophys. 362* (1), 1−11.
28. MacKerell, A. D., Bashford, D., Bellott, M., Dunbrack, R. L., Evanseck, J. D., Field, M. J., Fischer, S., Gao, J., Guo, H., Ha, S., McCarthy, D. J., Nguyen, D. T., Prodhom, B., Reiher, W. E., III, Roux, B., Schlenkrich, M., Smith, J. C., Stote, R., Straub, J., Watanabe, M., Kuczera, J. W., Yin, D., and Karplus, M. (1998) All-atom emipical potential for molecular modeling and dynamics studies of proteins, *J. Phys. Chem. B 102*, 3586−3616.
29. Marx, U. C., Adermann, K., Bayer, P., Forssmann, W. G., and Rosch, P. (2000) Solution structures of human parathyroid hormone fragments hpth(1−34) and hpth(1−39) and bovine parathyroid hormone fragment bpth(1−37), *Biochem. Biophys. Res. Commun. 267* (1), 213−220.
30. Meyer, J. D., Ho, B., and Manning, M. C. (2002) Effects of conformation on the chemical stability of pharmaceutically relevant polypeptides, in *Rational Design of Stable Protein Formulations* (Carpenter, F. J., and Manning, C. M., Eds.) pp 85−107, Kluwer Academic/Plenum Publishers, New York.
31. Nabichi, Y., Fujiwara, E., Kuboniwa, H., Asoh, Y., and Ushio, H. (1998) Kinetic study of methionine oxidation in human parathyoid hormone, *Anal. Chim. Acta 365*, 301−307.
32. Narhi, L. O., Kenney, W. C., and Arakawa, T. A. (1991) Conformational changes of recombinant human granulocyte conlony-stimulating factor, *J. Protein Chem. 10*, 359−367.
33. Nguyan, T. H. (1994) Oxidation degradation of protein pharmaceuticals, *ACS Symp. Ser.*, 59−71.
34. Nosé, S. (1991) Constant temperature molecular dynamic methods, *Prog. Theor. Phys. Suppl. 103*, 1−46.
35. Nyquist, R. M., Heitbrink, D., Bolwien, C., Gennis, R. B., and Heberle, J. (2003) Direct observation of protonation reactions

during the catalytic cycle of cytochrome *c* oxidase, *Proc. Natl. Acad. Sci. U.S.A. 100* (15), 8715−8720.
36. Pellegrini, M., Royo, M., Rosenblatt, M., Chorev, M., and Mierke, D. F. (1998) Addressing the tertiary structure of human parathyroid hormone-(1−34), *J. Biol. Chem. 273* (17), 10420−10427.
37. Potts, J. T., Kronenberg, H. M., and Rosenblatt, M. (1982) Parathyroid-hormone: chemistry biosynthesis, and mode of action, *Adv. Protein Chem. 35*, 323−396.
38. Powell, M. F. (1996) A compendium and hydropathy/flexibility analysis of common reactive sites in proteins: Reactivity at Asn, Asp, Gln, and Met motifs in neutral pH solution, in *Formulation, Characterization, and Stability of Protein Drugs: Case Histories* (Pearlman, R., and Wang, J. Y., Eds.) pp 1−140, Plenum Press, New York.
39. Ranky, W. O., and Nelson, D. C. (1961) Organic sulfur compounds, in *Organic sulfur compounds* (Kharasch, N., Ed.) p 170, Pergamon Press, New York.
40. Shahrokh, Z. (1997) Developing pharmaceutical protein formulations: Assumptions and analytical tools, *ACS Symp. Ser. 675*, 1.
41. Sömjen, D., Schlü×b9ter, K. D., Wingender, E., Mayer, H., and Kaye, A. M. (1991) Stimulation of cell-proliferation in skeletal tissues of the rat by defined parathyroid-hormone fragments, *Biochem. J. 277*, 863−868.
42. Strickland, L. A., Bozzato, R. P., and Kronis, K. A. (1993) Structure of human parathyroid hormone(1−34) in the presence of solvents and micelles, *Biochemistry 32* (23), 6050−6057.
43. Wang, W. (1999) Instability, stabilization, and formulation of liquid protein pharmaceuticals, *Int. J. Pharm. 185*, 129−188.
44. Wikstrom, M., Verkhovsky, M. I., and Hummer, G. (2003) Water-gated mechanism of proton translocation by cytochrome *c* oxidase, *Biochim. Biophys. Acta 1604* (2), 61−65.
45. Winer, K. K., Yanovski, J. A., and Cutler, G. B., Jr. (1996) Synthetic human parathyroid hormone 1−34 vs calcitriol and calcium in the treatment of hypoparathyroidism, *J. Am. Med. Assoc. 276* (8), 631−636.
46. Wishart, D. S., Bigam, C. G., Holm, A., Hodges, R. S., and Sykes, B. D. (1995) H-1, C-13 and N-15 random coil NMR chemical-shifts of the common amino acids. 1. Investigations of nearest-neighbor effects, *J. Biomol. NMR 5* (1), 67−81.
47. Wolff, S. P. (1993) Ferrous ion oxidation in the presence of ferric ion indicator xylenol orange for measurement of hydroperoxides, *Methods Enzymol. 233*, 182−189.
48. Zhang, Y. H., Feller, S. E., Brooks, B. R., and Pastor, R. W. (1995) Computer-simulation of liquid/liquid interfaces. 1. Theory and application to octane/water, *J. Chem. Phys. 103* (23), 10252−10266.

BI049151V